

## WARM HCN IN THE PLANET FORMATION ZONE OF GV TAU N

ASUNCIÓN FUENTE<sup>1</sup>, JOSÉ CERNICHARO<sup>2</sup>, MARCELINO AGÚNDEZ<sup>2,3,4</sup>

*Draft version September 28, 2018*

### ABSTRACT

The Plateau de Bure Interferometer has been used to map the continuum emission at 3.4 mm and 1.1 mm together with the  $J=1\rightarrow 0$  and  $J=3\rightarrow 2$  lines of HCN and  $\text{HCO}^+$  towards the binary star GV Tau. The 3.4 mm observations did not resolve the binary components and the HCN  $J=1\rightarrow 0$  and  $\text{HCO}^+$   $J=1\rightarrow 0$  line emissions trace the circumbinary disk and the flattened envelope. However, the 1.1 mm observations resolved the individual disks of GV Tau N and GV Tau S and allowed us to study their chemistry. We detected the HCN  $3\rightarrow 2$  line only towards the individual disk of GV Tau N, and the emission of the  $\text{HCO}^+$   $3\rightarrow 2$  line towards GV Tau S. Simple calculations indicate that the  $3\rightarrow 2$  line of HCN is formed in the inner  $R < 12$  AU of the disk around GV Tau N where the HCN/ $\text{HCO}^+$  abundance ratio is  $> 300$ . On the contrary, this ratio is  $< 1.6$  in the disk around GV Tau S. The high HCN abundance measured in GV Tau N is well explained by photo-chemical processes in the warm ( $> 400$  K) and dense ( $n > 10^7 \text{ cm}^{-3}$ ) disk surface.

*Subject headings:* ISM: individual objects (GV Tau N, GV Tau S) — ISM: lines and bands — radio continuum: ISM — stars:formation

### 1. INTRODUCTION

A fraction of the gas and dust in protoplanetary disks will end up in planets and may constitute the basis to form prebiotic species. A large effort has been done aiming to detect the warm gas in the planet formation zone using Spitzer and NIR ground-based facilities. In a pionering work, Lahuis et al. (2006) detected strong HCN and  $\text{C}_2\text{H}_2$  absorption features toward one source, IRS 46, from a sample of more than 100 Class I and II sources located in nearby star-forming regions. Later, Gibb et al. (2007, 2008) detected the HCN and  $\text{C}_2\text{H}_2$  absorption lines in GV Tau. Carr & Najita (2011) detected the rotational transitions of  $\text{H}_2\text{O}$  and OH and the rovibrational bands of simple organic molecules ( $\text{CO}_2$ , HCN,  $\text{C}_2\text{H}_2$ ) in 11 classical T Tauri stars showing that these molecules are not uncommon in the inner region of the T Tauri disks. Thus far, only NIR spectroscopy has provided information about the chemical composition of the gas in the inner disk region. Interferometric mm and submm observations are key to derive the kinematics and physical conditions of the gas, as well as the molecular abundance radial profiles that NIR studies cannot provide.

GV Tau (Haro 6-10) is a T Tauri binary system embedded in the L1524 molecular ( $d=140$  pc) cloud. It is one of a small number of young binaries for which the primary (GV Tau S) is optically visible and the companion (GV Tau N), located  $1.2''$  to the North, is strongly embedded. It is associated with a parsec-scale Herbig-Haro flow which extends to  $1.6$  pc to the north at a position angle of about  $222^\circ$  and  $\sim 1$  pc to the south (Devine et al. 1999; see also Movsessian & Magakian 1999). This region has been extensively studied in the NIR and all the studies pointed to the existence of a complex system composed of two circumstellar disks associated with GV Tau N and GV Tau S respectively that are themselves surrounded by a circumbinary disk and/or flattened nebula (Ménard et al.

1993, Koresko et al. 1999, Leinert et al. 2001). Doppmann et al. (2008) and more recently Wilking et al. (2012) proposed that GV Tau N and possibly GV Tau S could be binary systems themselves. The two individual disks GV Tau N and GV Tau S are misaligned and present different inclination angles. The GV Tau N disk has an edge-on geometry, while the GV Tau S disk is closer to a face-on orientation which allows the stellar radiation to escape forming a visible nebula (Roccatagliata et al. 2011). Only the GV Tau N disk has been detected in the  $\text{H}_2$   $2.12 \mu\text{m}$  ro-vibrational line (Herbst et al. 1995). The HCN and  $\text{C}_2\text{H}_2$  absorption ro-vibrational lines are detected towards GV Tau N (Gibb et al. 2007, 2008) which proves the existence of a rich organic chemistry in the inner disk of this star. The non-detection of these lines towards GV Tau S did not allow, however, to conclude about its disk chemistry since it could be due to the different disk inclination.

We present 3.4 mm and 1.1 mm interferometric images of GV Tau using the IRAM Plateau de Bure Interferometer (PdBI). The highest spatial resolution observations at 1.1 mm allowed us to resolve the GV Tau N and GV Tau S individual disks and have a first glance of the chemical differences between them.

### 2. OBSERVATIONS

The HCN  $1\rightarrow 0$  and  $\text{HCO}^+$   $1\rightarrow 0$  lines were observed using the PdBI in its CD configuration during 2009 October-November. This configuration provided an angular resolution of  $3.07'' \times 3.05''$  PA  $17^\circ$  ( $\sim 432 \text{ AU} \times 429 \text{ AU}$  at the distance of Taurus). During the observations two 40 MHz bandwidth correlator units were placed at the frequencies of the HCN  $1\rightarrow 0$  (88631.85 MHz) and  $\text{HCO}^+$   $1\rightarrow 0$  (89188.52 MHz) lines providing a spectral resolution of 78 kHz. These lines were also observed with the 320 MHz units which provided a spectral resolution of  $\sim 2.5$  MHz. Other two 320 MHz units were placed in a frequency range free of lines to measure the continuum and subtract it from the spectral line maps.

In 2011 February, we performed sub-arcsecond imaging of this region in the HCN  $3\rightarrow 2$  and  $\text{HCO}^+$   $3\rightarrow 2$  lines using the PdBI in its A configuration, which provides a beam of  $\sim 0.49'' \times 0.26''$  PA  $16^\circ$  ( $\sim 69 \text{ AU} \times 36 \text{ AU}$ ). Two 40 MHz

a.fuente@oan.es

<sup>1</sup> Observatorio Astronómico Nacional (OAN,IGN), Apdo 112, E-28803 Alcalá de Henares, Spain

<sup>2</sup> Centro de Astrobiología (CSIC/INTA), Laboratory of Molecular Astrophysics, Ctra. Ajalvir km. 4, E-28850, Torrejón de Ardoz, Spain

<sup>3</sup> Univ. Bordeaux, LAB, UMR 5804, F-33270, Floirac, France

<sup>4</sup> CNRS, LAB, UMR 5804, F-33270, Floirac, France

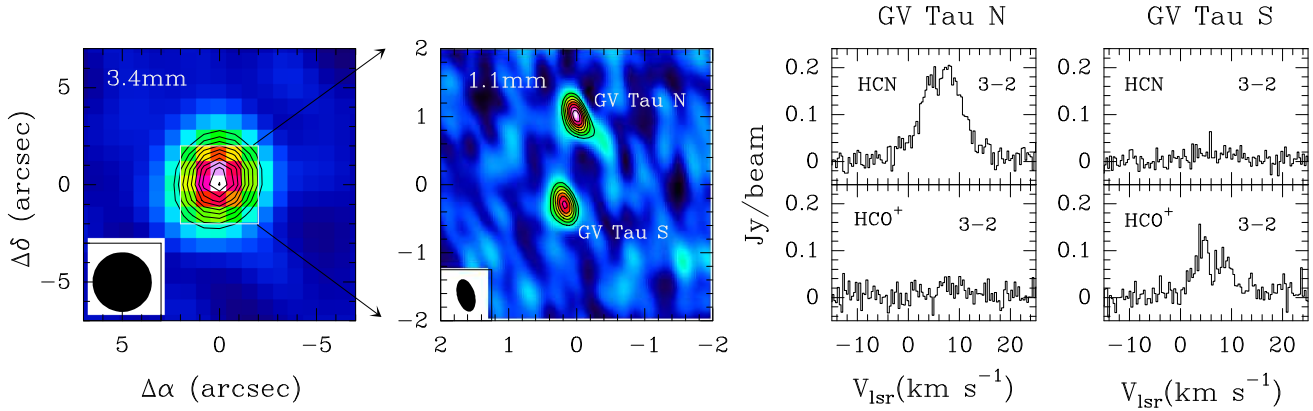


FIG. 1.— *Right panel:* Interferometric image of the continuum emission at 3.4 mm. Contour Levels are 3 mJy/beam to 13 mJy/beam by 1 mJy/beam. The image is centered at RA(J2000)=04:29:23.73 Dec(J2000)=24:33:00.30. *Central panel* Interferometric image of the continuum emission at 1.1 mm. Contour Levels are 10 mJy/beam to 50 mJy/beam by 5 mJy/beam. *Left panel* Interferometric spectra of the HCN 3→2 and HCO<sup>+</sup> 3→2 lines towards GV Tau N and GV Tau S.

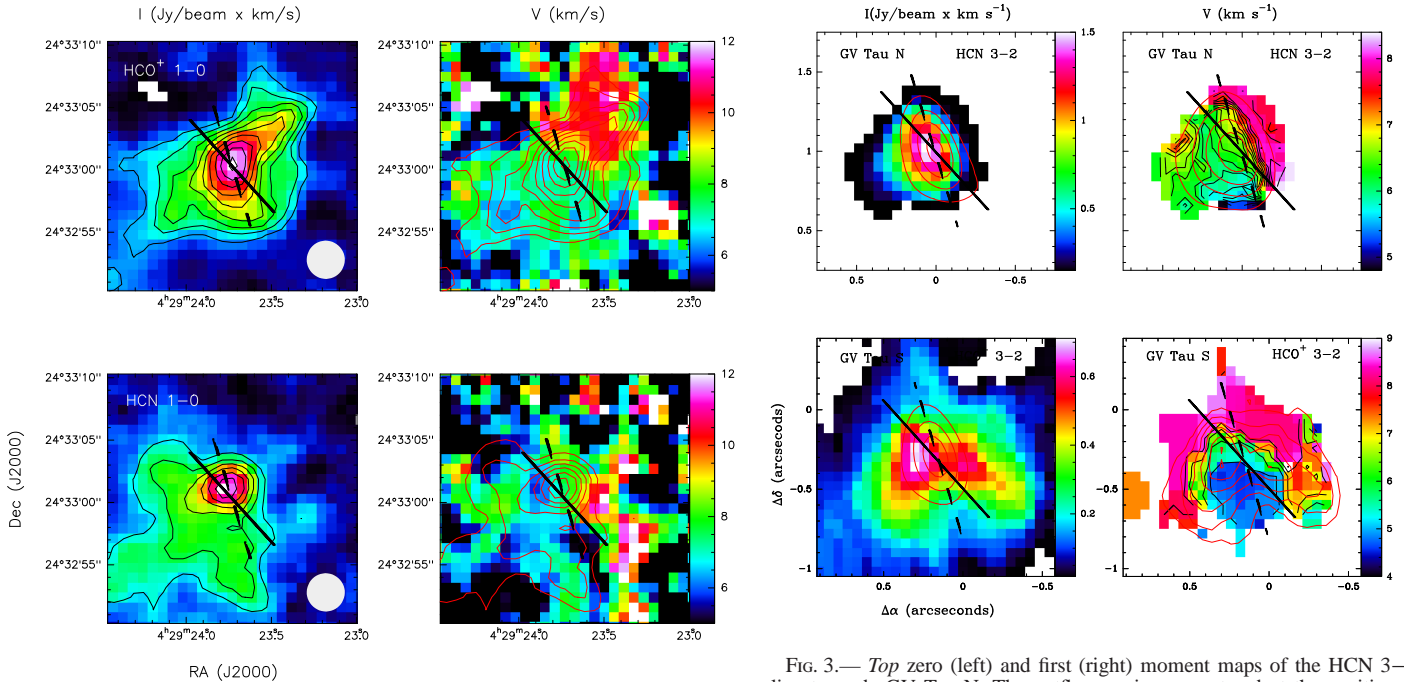


FIG. 2.— *Top* zero (left) and first (right) moment maps of the HCO<sup>+</sup> 1→0 line towards GV Tau. Contour levels are 0.1 to 0.5 by 0.05 Jy/beam×km s<sup>-1</sup>. The directions of the large scale outflow defined by the giant Herbig Haro flow (PA=222°; Devine et al. 1999) and of the Herbig-Haro jet (PA=195°; Movsessian & Magakian 1999) are indicated by two black lines through the phase center. *Bottom* the same for the HCN 1→0 line.

correlator units were placed at the frequencies of the HCN 3→2 (265886.18 MHz) and HCO<sup>+</sup> 3→2 (267557.526 MHz) lines. We used the correlator WIDEX to cover the 4 GHz bandwidth of the receivers (264.58 - 268.18 GHz). Only HCO<sup>+</sup> 3→2 and HCN 3→2 were detected down to an rms of 6 mJy/beam with a spectral resolution of 2 MHz. The channels without line emission in WIDEX were used to create the continuum 1.1 mm map which was subtracted from the spectral maps. The resulting 3.4 mm and 1.1 mm continuum images are shown in Fig. 1. The spectral maps are shown in Fig. 2 and Fig. 3. The phase center in our observations was RA(J2000)=04:29:23.73 Dec(J2000)=24:33:00.30, in between the two stars.

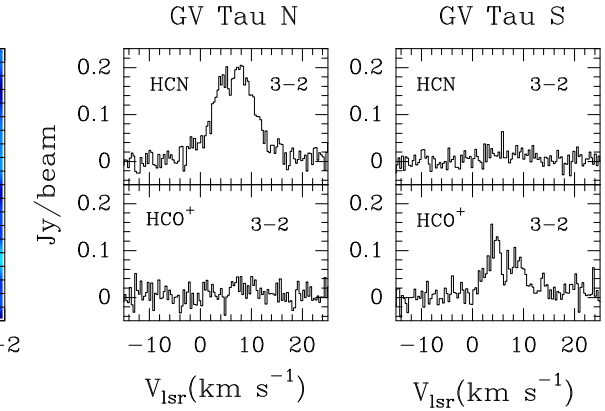


FIG. 3.— *Top* zero (left) and first (right) moment maps of the HCN 3→2 line towards GV Tau N. The outflows axis are centered at the position of GV Tau N (04:29:23.731, 24:33:01.30). In the left panel, the red contours correspond to the continuum 1.1 mm image and contour levels are 0.01 to 0.04 by 0.01 Jy/beam. In the right panel, red contours correspond to the integrated intensity of the HCN 3→2 line and contour levels are 0.150 to 1.5 by 0.150 Jy/beam×km s<sup>-1</sup>. *Bottom* the same for the HCO<sup>+</sup> 3→2 line. The outflow axes are centered at the position of GV Tau S (04:29:23.743, 24:32:59.99). Contours in the left panel are 0.1 to 0.7 by 0.1 Jy/beam×km s<sup>-1</sup>.

### 3. RESULTS

#### 3.1. Continuum

Our 3.4 mm image does not resolve the two components of the binary. An elliptical Gaussian was fit to the uv table and the parameters are shown in Table 1. The size of the emission, ~280 AU in diameter, is slightly smaller than the size of the NIR nebula observed by Ménard et al. (1993). The 3.4 mm continuum emission peaks in the middle of the two stars, suggesting a similar contribution to the total flux from the two disks. The total flux,  $16.1 \pm 0.4$  mJy is consistent with that measured by Guilloteau et al (2011).

Our 1.1 mm observations clearly resolve the two components which present similar intensity. Gaussian fits to the uv tables were done and the parameters are shown in Table 1. Because of our elongated beam, the disks are resolved in only one direction. Our fit gives a radius of  $\sim 0.07''$  ( $\sim 10$  AU) for the emission of the two disks. Guilloteau et al. (2011) observed this target using the PdBI with a larger beam of  $0.89'' \times 0.56''$  and derived a size twice larger than ours. After modeling the emission, they concluded that the two disks are, very likely, optically thick and the size was overestimated because of the atmospheric seeing. This could be a reason for our disagreement. Another possibility is that we have filtered out part of the disk emission. The filtering effect would be more severe towards GV Tau S disk because of the face-on orientation. With the sizes derived from our observations, we estimate a brightness temperature of  $>69$  K for the N and  $>56$  K for the S components respectively (we give a lower limit because the emission is essentially unresolved in one direction), consistent with the emission arising from the  $R < 10$  AU region of a T Tauri disk (Pinte et al. 2006).

### 3.2. Spectral Observations

We have detected intense emission of the HCN  $1 \rightarrow 0$  and  $\text{HCO}^+$   $1 \rightarrow 0$  lines towards GV Tau. The integrated emission of the  $\text{HCO}^+$   $1 \rightarrow 0$  line is composed of a compact source centered at the phase center and an envelope elongated in the south-east north-west direction. In Fig. 2 we show the velocity map of the  $\text{HCO}^+$   $1 \rightarrow 0$  line. A clear velocity gradient is detected in the south-east north-west direction. The direction of this gradient is close to orthogonal to the main Herbig Haro outflow, and consistent with the existence of a rotating circumbinary disk. The integrated emission of the HCN  $1 \rightarrow 0$  line is composed of a compact source and an extended envelope. The compact source peaks  $\sim 1''$  to the North of the phase center suggesting a larger contribution of GV Tau N to the total emission. The extended emission is very asymmetric, being more extended towards the south-east than towards the north-west. Moreover, the HCN  $1 \rightarrow 0$  emission has an elongation in the outflow direction (see Fig. 2). There is some hint of velocity gradient in the HCN  $1 \rightarrow 0$  line although in this case the gradient is less clear than in the case of  $\text{HCO}^+$   $1 \rightarrow 0$ .

In Fig. 1 we show the spectra of the HCN  $3 \rightarrow 2$  and  $\text{HCO}^+$   $3 \rightarrow 2$  lines towards GV Tau N and S. The HCN  $3 \rightarrow 2$  line is only detected towards the N component. The  $\text{HCO}^+$  line is clearly detected towards the S component and tentatively detected towards the N. The velocity integrated intensity map of the HCN  $3 \rightarrow 2$  line is well fitted with an elliptical Gaussian of  $0.32 \pm 0.04'' \times 0.25 \pm 0.05''$  centered at the star position, a size slightly larger than that of the 1.1 mm continuum emission. The emission of the  $\text{HCO}^+$   $3 \rightarrow 2$  line is clearly more extended than the 1.1 mm continuum suggesting some contribution from the circumbinary disk and/or the nebula. Fitting an elliptical Gaussian in the uv plane, we obtain a size of  $1.26 \pm 0.06'' \times 0.73 \pm 0.09''$ . The zero and first momentum maps of the HCN  $3 \rightarrow 2$  and  $\text{HCO}^+$   $3 \rightarrow 2$  line emissions are shown in Fig. 3. A clear velocity gradient is detected in GV Tau N. The velocity gradient defines a rotation axis that is in between that of the main Herbig Haro outflow and the Herbig jet (Devine et al. 1999, Movsessian & Magakian 1999). In GV Tau S we detect a velocity gradient in the north-south direction but it cannot be interpreted as a disk rotation. The kinematics of the  $\text{HCO}^+$   $3 \rightarrow 2$  line is very likely affected by the outflow motion.

### 3.3. HCN and $\text{HCO}^+$ Column Densities

Gibb et al. (2007, see also erratum 2008) detected absorption due to the HCN  $\nu_3$  towards GV Tau N. The estimated column density and rotational temperature were  $3.7 \pm 0.3 \times 10^{16} \text{ cm}^{-2}$  and  $115 \pm 10$  K for HCN assuming a linewidth of  $12 \text{ km s}^{-1}$ . With these physical conditions the HCN  $3 \rightarrow 2$  line is optically thick and the expected brightness temperature is  $\sim 110$  K. We measured a peak intensity of  $192 \text{ mJy/beam}$  ( $\sim 26$  K) towards GV Tau N which implies that the size of the emitting region is  $< 24$  AU, so that the warm HCN is present in the inner  $R < 12$  AU from the star. The HCN  $3 \rightarrow 2/\text{HCO}^+$   $3 \rightarrow 2$  flux ratio towards GV Tau N is  $\sim 10$ . LVG calculations show that assuming that both molecules arise in the same region with the physical conditions derived by Gibb et al. (2007), the HCN/ $\text{HCO}^+$  column density ratio is  $\sim 300$  (see Fig. 4a). The brightness temperature of the HCN  $1 \rightarrow 0$  line in this small region would then be  $\sim 94$  K, which diluted in the 3.4 mm beam would give a main beam brightness temperature of  $< 0.28$  K. The main beam brightness temperature we measure is larger,  $\sim 0.85$  K, consistent with the fact that the emission is extended and mostly arises from the outer part of the disk and the circumbinary disk/nebula.

Towards GV Tau S, only the  $\text{HCO}^+$   $3 \rightarrow 2$  line is well detected and the HCN  $3 \rightarrow 2/\text{HCO}^+$   $3 \rightarrow 2$  flux ratio is  $< 0.3$ . Assuming  $n(\text{H}_2) = 10^7 \text{ cm}^{-3}$  and a kinetic temperature of  $\sim 18$  K, we derive a beam averaged column density of  $N(\text{HCO}^+) = 1.0 \times 10^{14} \text{ cm}^{-2}$  in a linewidth of  $8.6 \text{ km s}^{-1}$  and the HCN/ $\text{HCO}^+$  column density ratio would be  $< 0.6$  (see Fig. 4a). Other possibility is that the emission arise in the lower density and warmer disk surface. In Fig. 4a, we explored this possibility ( $n(\text{H}_2) = 10^5 \text{ cm}^{-3}$ ,  $T_k = 115$  K) and conclude that in this case we would obtain  $N(\text{HCN})/N(\text{HCO}^+) < 1.6$ .

We use the 3.4 mm lines of HCN and  $\text{HCO}^+$  to have an estimate of the HCN/ $\text{HCO}^+$  column density ratio in the nebula surrounding the binary. Using the integrated line intensity of the weakest satellite component of the HCN  $1 \rightarrow 0$  line, assuming Local Thermodynamic Equilibrium and  $T_{\text{rot}} = 15$  K, we estimate a beam averaged column density of  $1.7 \times 10^{13} \text{ cm}^{-2}$ . With the same assumptions, we derive a  $\text{HCO}^+$  column density of  $\approx 1 \times 10^{13} \text{ cm}^{-2}$ . Therefore the average HCN/ $\text{HCO}^+$  column density in this region is  $\approx 1.7$ . This ratio is not dependent on the assumed rotation temperature as long as it is the same for the two molecules, which is a reasonable assumption taking into account their similar dipole moments.

## 4. DISCUSSION AND CONCLUSIONS

Our millimeter data allow for the first time to sample the planet formation zone of the disks GV Tau N and GV Tau S and evidence a dramatic chemical differentiation in the molecular gas associated with GV Tau N and GV Tau S. Previous NIR observations did not allow to conclude because the absorption lines are strongly dependent on the disk orientation. Our observations show that the HCN/ $\text{HCO}^+$  ratio must be  $> 300$  in the planet formation zone of GV Tau N. In contrast, the HCN/ $\text{HCO}^+$  must be  $< 1.6$  in GV Tau S. The huge HCN column density found in the inner  $R < 12$  AU disk of GV Tau N is consistent with the chemical calculations by Agúndez-Cernicharo & Goicoechea (2008). They predicted an HCN abundance as large as  $5 \times 10^{-5}$  in the inner  $R < 3$  AU of circumstellar disks (see Fig. 4b). The HCN is not arising from the disk mid-plane but from the photon-dominated region in the disk surface. The high densities and temperatures in this region are essential to achieve a huge HCN abundance (Cernicharo 2004). The synthesis of organic molecules in the gas requires that atomic carbon, produced by the dissociation of  $\text{CO}$ , in-



TABLE 1  
GAUSSIAN FITS TO THE CONTINUUM AND SPECTRAL DATA

Source	$\lambda$	HPBW(")	Flux (mJy)	Major (")	Minor (")	PA	
GV Tau N+S	04:29:23.733 24:33:00.56	3.4mm <sup>1</sup>	3.07"×3.05"	16.1 (0.4)	2.02 ( 0.08)	1.06 ( 0.13)	-14 (3)
GV Tau N	04:29:23.731 24:33:01.30	1.1mm <sup>1</sup>	0.49"×0.26"	49.8 ( 1.1)	0.14 ( 0.03)	0.03 (0.04)	52 (1)
		1.3mm <sup>2</sup>	0.89"×0.56"	43.8 (3.1)	0.24 (0.11)	0.09 (0.06)	53 (18)
		HCN 3→2 <sup>1</sup>	0.50"×0.25"	3.64(0.21) <sup>3</sup>	0.32(0.04)	0.25(0.05)	-41(20)
GV Tau S	04:29:23.743 24:32:59.99	1.1mm <sup>1</sup>	0.49"×0.26"	38.0 ( 1.1)	0.12 ( 0.02)	0.03 (0.05)	-34 (1)
		1.3mm <sup>2</sup>	0.89"×0.56"	46.7 (3.2)	0.37 (0.05)	0.11 (0.07)	-2(8)
		HCO <sup>+</sup> 3→2 <sup>1</sup>	0.49"×0.28"	9.24(1.1) <sup>3</sup>	1.26(0.06)	0.73(0.09)	-74(5)

<sup>1</sup> This work; <sup>2</sup> Guilloteau et al. (2011); <sup>3</sup> Total flux in Jy×km s<sup>-1</sup>.

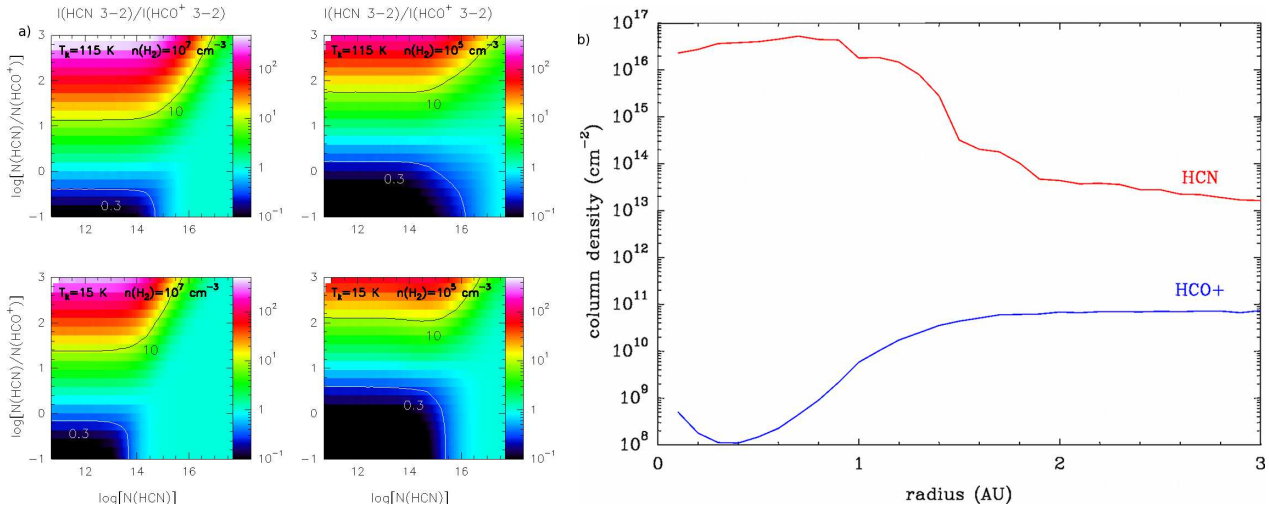


FIG. 4.— **a)** Plots of the HCN 3→2/HCO<sup>+</sup>3→2 line intensity ratio,  $I(\text{HCN}3\rightarrow 2)/I(\text{HCO}^+3\rightarrow 2)$  as a function of the HCN column density in a linewidth of 10 km s<sup>-1</sup> and the HCN/HCO<sup>+</sup> abundance ratio for different physical conditions. The calculations have been done using the LVG code MADEX (J. Cernicharo 2012). Contour levels for the values found in GV Tau N, 10, and GV Tau S, 0.3, are drawn. **b)** HCN and HCO<sup>+</sup> vertical column densities calculated with the model described in Agúndez, Cernicharo & Goicoechea (2008) in the PDR within the inner 3 AU of a protoplanetary disk around a T Tauri star. They are computed by integrating the gas molecular densities from the inner height  $z_{in}$  ( $A_v < 2$ ) to the disk surface.

incorporates into C-bearing species faster than reverting to CO. For example, C<sub>2</sub>H<sub>2</sub> and HCN reach low abundances at 100 K because the reactions of C<sub>2</sub>H and CN with H<sub>2</sub> have activation barriers (Cernicharo 2004). At temperatures above ~400 K atomic oxygen is efficiently converted into OH, which may react with C to form CO but reacts faster with H<sub>2</sub> to form water. Thus, most of the oxygen forms H<sub>2</sub>O, and CO does not reach its maximum abundance allowing atomic carbon to form C-bearing molecules. The key reactions for the HCN formation such that C+NO→CN+O, or H<sub>2</sub>+CN→HCN+H, proceed very rapidly at these large gas densities (>10<sup>7</sup> cm<sup>-3</sup>) and temperatures (Cernicharo 2004). This mechanism also works for any dense PDR such as those found around protoplanetary nebula where the photodissociation of CO and HCN allows a fast photo-polymerization towards longer carbon chains (Cernicharo 2004). This same result was found by Walsh et al. (2010) in their disk chemical model which included a grain-surface network. In that model the [HCN]/[HCO<sup>+</sup>] ratio was

~1000 at R~1 AU and always >10 for R<10 AU. Although not essential, accretion shocks could contribute to enhance the density and gas kinetic temperature and make the HCN formation more efficient.

One puzzling question then is the non-detection of HCN in GV Tau S. This can only be explained by a different disk morphology (flatter disk, an inner gap), different dust properties and/or a different gas/dust ratio in the inner disk. Higher spatial resolution interferometric observations are required to unveil the hidden structure of this interesting binary.

This project has been partially supported within the program CONSOLIDER INGENIO 2010, under grant CSD2009-00038 "Molecular Astrophysics: The Herschel and ALMA Era ASTROMOL". We also thank the Spanish MICINN for funding support through grants AYA2006-14876 and AYA2009-07304.

## REFERENCES

- Agúndez, M., Cernicharo, J., & Goicoechea, J. R. 2008, A&A, 483, 831  
 Carr, J. S., & Najita, J. R. 2011, ApJ, 733, 102  
 Cernicharo, J., 2004, ApJ, 608, L41  
 Cernicharo, J., 2012, ECLA-2011: Proceedings of the European Conference on Laboratory Astrophysics, European Astronomical Society Publications Series, 2012, Editors: C. Stehlé, C. Joblin and L. d'Hendecourt  
 Devine, D., Reipurth, B., Bally, J., & Balonek, T. J. 1999, AJ, 117, 2931  
 Doppmann, G. W., Najita, J. R., & Carr, J. S. 2008, ApJ, 685, 298  
 Gibb, E.L., Van Brunt, K.A., Brittain, S.D., & Rettig, T.W., 2007, ApJ, 660, 1572  
 Gibb, E.L., Van Brunt, K.A., Brittain, S.D., & Rettig, T.W., 2008, ApJ, 686, 748

- Guilloteau, S., Dutrey, A., Piétu, V., & Bohler, Y. 2011, *A&A*, 529, A105  
Herbst, T. M., Koresko, C. D., & Leinert, C. 1995, *ApJ*, 444, L93  
Koresko, C. D., Blake, G. A., Brown M.E., et al., 1999, *ApJ*, 525, L49  
Lahuis, F., van Dishoeck, E. F., Boogert, A. C. A., et al. 2006, *ApJ*, 636, L145  
Leinert, C., Beck, T. L., Ligi, S., et al. 2001, *A&A*, 369, 215  
Ménard, F., Monin, J.-L., Angelucci, F., & Rouan, D. 1993, *ApJ*, 414, L117  
Movsessian, T. A., & Magakian, T. Y. 1999, *A&A*, 347, 266  
Pinte, C., Ménard, F., Duchêne, G., & Bastien, P. 2006, *A&A*, 459, 797  
Roccatagliata, V., Ratzka, T., Henning, T., et al. 2011, *A&A*, 534, A33  
Walsh, C., Millar, T. J., & Nomura, H. 2010, *ApJ*, 722, 1607  
Wilking, B. A., Marvel, K. B., Claussen, M. J., et al. 2012, *arXiv:1205.5760*